RESEARCH ARTICLE | MAY 24 2016

Linear chirped slope profile for spatial calibration in slope measuring deflectometry

F. Siewert; T. Zeschke; T. Arnold; H. Paetzelt; V. V. Yashchuk

Rev. Sci. Instrum. 87, 051907 (2016)
https://doi.org/10.1063/1.4950737

Linear chirped slope profile for spatial calibration in slope measuring deflectometry

F. Siewert,[1,a] T. Zeschke,[1] T. Arnold,[2] H. Paetzelt,[2] and V. V. Yashchuk[3]
[1]*Helmholtz Zentrum Berlin für Materialien und Energie, Institut für Nanometer Optik und Technologie, Albert-Einstein-Str. 15, 12489 Berlin, Germany*
[2]*Leibnitz Institut für Oberflächen Modifizierung Leipzig e.V., IOM, Permoserstr. 15, 04318 Leipzig, Germany*
[3]*Lawerence Berkeley National Laboratory, Advanced Light Source, 1 Cyclotron Road, Berkeley, California 94720, USA*

(Received 22 December 2015; accepted 22 March 2016; published online 24 May 2016)

Slope measuring deflectometry is commonly used by the X-ray optics community to measure the long-spatial-wavelength surface figure error of optical components dedicated to guide and focus X-rays under grazing incidence condition at synchrotron and free electron laser beamlines. The best performing instruments of this kind are capable of absolute accuracy on the level of 30-50 nrad. However, the exact bandwidth of the measurements, determined at the higher spatial frequencies by the instrument's spatial resolution, or more generally by the instrument's modulation transfer function (MTF) is hard to determine. An MTF calibration method based on application of a test surface with a one-dimensional (1D) chirped height profile of constant amplitude was suggested in the past. In this work, we propose a new approach to designing the test surfaces with a 2D-chirped topography, specially optimized for MTF characterization of slope measuring instruments. The design of the developed MTF test samples based on the proposed linear chirped slope profiles (LCSPs) is free of the major drawback of the 1D chirped height profiles, where in the slope domain, the amplitude strongly increases with the local spatial frequency of the profile. We provide the details of fabrication of the LCSP samples. The results of first application of the developed test samples to measure the spatial resolution of the BESSY-NOM at different experimental arrangements are also presented and discussed. [http://dx.doi.org/10.1063/1.4950737]

I. INTRODUCTION

X-ray mirrors and gratings as used in synchrotron application or X-ray astronomy are usually specified in terms of slope error to characterize the low-spatial frequency error (LSFE) covered by the spatial wavelength range from about 1 to 2 mm up to the full aperture length. Slope measuring systems enable the inspection of reflective surfaces by direct measurement of the deflection angle of a probing laser beam. They allow an uncomplicated inspection of reflective surfaces of different shape such as a plane, sphere, toroid, and ellipse. For the case of the last mentioned x-ray mirrors, local curvature on the clear aperture is usually in the range of a few meters to some 10 m and even larger in case of focusing mirrors at Free Electron Lasers (FELs). The allowed local deviations from an ideal shape are usually in the range of a few nanometers. X-ray mirrors are used under grazing incidence condition[1,2] and show a specific clear aperture size: long aperture length in meridional direction and short width in sagittal orientation. Thus a line-scan as performed with a slope measuring profiler is in most cases sufficient to characterize the optics shape.

Since the late 1980's, slope measuring instruments like the well-known Long Trace Profiler (LTP)[3,4] and the Nanometer Optic component measuring Machine (NOM)[5,6] have been used to measure the LSFE of optical elements. Autocollimator-based slope measuring profilers[7–13] as well as upgraded LTP's[14–17] provide sub 100 nrad root mean square (rms) accuracy for measuring long flat and slightly curved optical components.[18,19] Dedicated mapping techniques enable complete characterizing of optical components' 3D topography.[20,21] Past experience has shown that a careful characterization and calibration of slope measuring profilers is essential to achieve the accuracy requirements for the synchrotron optics of today.[22–24] The spatial resolution achievable by slope measuring deflectometry is of special importance, mainly in the case when topography data are used to simulate the performance of optical components[25,26] or when deterministic surface finishing is applied to remove residual figure deviations.[27–29] For such use, a precise spatial frequency calibration is essential. In past publications, it was proposed to characterize such devices with dedicated test samples of periodic and chirped profiles.[22,30] First experimental work on this topic was published in 2013,[31] showing the suitability of this approach. In this work, we suggest and develop the samples with a 2D-chirped topography specially optimized to characterize the performance of slope measuring profilers in terms of spatial resolution and the modulation transfer function (MTF).

[a]Author to whom correspondence should be addressed. Electronic mail: frank.siewert@helmholtz-berlin.de.

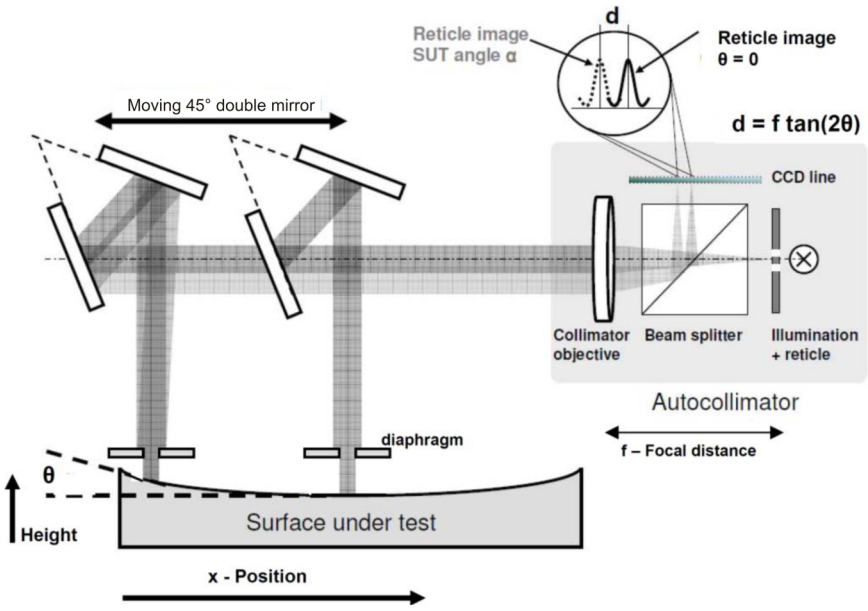

FIG. 1. Principle setup of a slope measuring profiler with scanning 45°-double-mirror as realized for the BESSY-NOM.

II. THE PRINCIPLE OF SLOPE MEASURING DEFLECTOMETRY

Figure 1 shows the optical setup of a slope measuring profiler as realized at the BESSY-NOM for a fixed optics-head (autocollimator) with a movable 45°-double mirror setup for guiding the test beam.[21] The laser test light beam [$\lambda = 650$ nm generated by a light-emitting diode (LED)] is traced at regular intervals over the mirror along the line of inspection. Different investigations in the past have shown a measurement beam diameter of 2.5 mm to be the optimal size in the case of a plane or slightly curved optics under inspection.[21,31] With this arrangement, reflective surfaces of plane and curved shape down to local radius of curvature of R = 3.5 m can be measured. Measuring strongly curved optical elements with radii smaller than R = 20 m down to R = 3.5 m local curvature beam diameter of 0.8 mm can be applied. A diaphragm placed at a distance of 3 mm from the optics under test defines the size of the measuring beam, see Fig. 1. Depending on the local topography of surface under test (SUT), the test beam will be reflected into the position sensitive detector of the NOM autocollimator head. Its position on the CCD-line of the sensor is directly related to the local surface slope, see Fig. 1. The reflection of the test beam along the optical axis of the instrument is determined by the angle between the mirror normal and the direction of the impinging laser beam.[32,33] Then the local slope is given by

$$S(x) = \tan\theta = dy/dx. \tag{1}$$

The relative slope change is measured by scanning along the line of inspection. The sensor detects the change of the angle of reflection from one position x on the mirror substrate to the next position $x + \Delta x$. A spatial integration of the slope data finally gives the topography height profile $h(x_k)$

$$h(x_k) = h(x_0) + \sum_{m=1}^{k} \frac{dx}{2}\left[S(x_m) + S(x_{m-1})\right]. \tag{2}$$

The size of the beam limited diaphragm is the major factor that defines the instrument's spatial resolution. However, the exact value of the resolution depends also on the diaphragm shape, its position with respect to the SUT, and other peculiarities of the measurement arrangement. In this work, we suggest and demonstrate a new approach to reliably measure the spatial resolution and modulation transfer function of surface slope profilometers. The approach is based on application of a specially designed chirped profile; see Secs. III and IV below.

III. DESIGN CONSIDERATIONS FOR CHIRPED PROFILES FOR SPATIAL CALIBRATION

In previous work, we have demonstrated the suitability of chirped surface slope profiles for spatial frequency calibration in general. In Ref. 31, a chirped profile with a constant height distribution h given by

$$h = amplitude \cdot \cos(2\pi \cdot position/P(position)) + amplitude, \tag{3}$$

where the amplitude parameter is $amplitude = 2.5$ nm and the function $P(position)$ is

$$P(position) = 0.3 + 0.043\,75 \cdot \sqrt{50 \cdot position}. \tag{4}$$

The position is given in millimeters.

This type of chirped sample was designed to fulfill the requirement to have low figure deviations of the profile's amplitude of about 10-nm peak-to-valley (pv), which corresponds to figure deviations typical for real synchrotron optics. Tests with this sample at the BESSY-NOM have shown that a spatial resolution of about 1.7 mm is achieved with a beam diameter of 2.5 mm.[31] The measured value of the resolution is in excellent agreement to theoretical estimations from ARMA modelling of data[34] measured with the Developmental Long Trace Profiler (DLTP) at Lawrence Berkeley National Lab[8] also equipped with 2.5 mm beam limiting diaphragm.

However, chirped profiles of constant height amplitude described above show some drawbacks. The dependence of the frequency shift on position is strongly nonlinear and varies from about 5% at the highest frequency to approximately 100% at the lowest frequency. An additional drawback of a chirped constant-height specified by Eqs. (3) and (4) is an approximately linear increase of the slope amplitude with increase of the spatial frequency, and therefore, a sharp change (due to the dependence of the frequency on the position mentioned above) of the slope amplitude along the sample. These strong variations together with the effective superposition of two chirped profiles in the slope domain [that can be seen by differentiating Eq. (3)] can make difficult numerical interpretation of the results of measurements with the sample in the terms of the instrumental MTF. Uncertainty of the interpretation can also be caused by possible errors in finding the frequency shift correction due to the limited tolerances of fabrication in the chirped profile.

Based on the consideration above, as an optimization requirement to the design of a chirped profile suitable for slope measurements, we suggest constant (independent of lateral position) amplitude in the slope domain rather than in the height domain. The goal with this new design is to avoid the frequency doubling effect and other problems characteristic to the constant-height-amplitude sample discussed above. The desired chirped slope test sample with the constant slope amplitude A_0 and with a linear variation of spatial frequency, $f(x) = 2\pi(\omega_0 + \omega_1 \cdot x)$, seems to be the most preferable from the point of view of uniform representation of different spatial frequencies

$$\alpha(x) = A_0 \cdot \sin\left[2\pi(\omega_0 + \omega_1 \cdot x) \cdot (x + x_0)\right]. \tag{5}$$

In Eq. (5), the argument of the sin function is described with three parameters, ω_0, ω_1, and x_0, constant with the general form of a second order polynomial,

$$\phi(x) = 2\pi(\omega_0 + \omega_1 \cdot x + \omega_1 \cdot x^2). \tag{6}$$

The corresponding height profile $h(x)$ is determined by direct integration of Eq. (5) and leads to the following expression:

$$h(x) = \frac{A_0}{2\sqrt{\omega_1}} \cdot \left\{\cos\,\phi_0 \cdot S\left[\frac{\omega_0 + \omega_1 \cdot (2x + x_0)}{\sqrt{\omega_1}}\right] + \sin\phi_0 \cdot C\left[\frac{\omega_0 + \omega_1 \cdot (2x + x_0)}{\sqrt{\omega_1}}\right]\right\}, \tag{7}$$

where the functions $S[x]$ and $C[z]$ are Fresnel integrals defined through the following integral representations:

$$S[z] = \int_0^z \sin(z^2)dz \;\text{ and }\; C[z] = \int_0^z \cos(z^2)dz, \tag{8}$$

and the phase φ_0 is

$$\varphi_0 = \frac{\pi(\omega_0 - \omega_1 \cdot x_0)^2}{2\omega_1}. \tag{9}$$

According to the definition in (8), the two terms in (7) are different only by a phase shift of $\pi/2$ in the trigonometric function of the Fresnel integrals (9). Therefore, without loss of generality, we can reduce (7) to the first term by zeroing the phase φ_0 *via* setting

$$\omega_0 = \omega_1 \cdot x_0. \tag{10}$$

Then, in the height domain, the simplified constant-slope chirped profile with linear frequency distribution is

$$h(x) = \frac{A_0}{2\sqrt{\omega_1}} \cdot S\left[2\sqrt{\omega_1} \cdot (x + x_0)\right]. \tag{11}$$

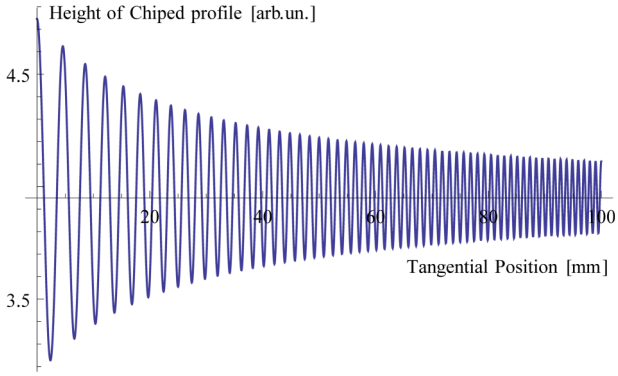

FIG. 2. Appearance of linear chirped profile (11) with parameters $A_0 = 1$, $\omega_1 = 0.004$ mm^{-2}, and $x_0 = 25$ mm in the height domain.

Figure 2 shows a profile according to Eq. (11) with the parameters: $A_0 = 1$ arbitrary units, $\omega_1 = 0.004$ mm^{-2}, and $x_0 = 25$ mm in the interval of lateral position of $x \in [0, 100]$ mm.

The corresponding linear chirped profile in the slope domain is determined by differentiating Eq. (11)

$$\alpha(x) = A_0 \cdot \sin\left[2\pi\omega_1 \cdot (x + x_0)^2\right]. \tag{12}$$

In Fig. 3, the optimized chirp profile is depicted in the slope domain as prescribed in Eq. (12).

IV. SPECIFICATION OF OPTIMIZED CHIRP PROFILE FOR SPATIAL RESOLUTION CALIBRATION

Based on the consideration above, we suggest the linear chirped slope profiles (LCSPs) with linear variation of spatial frequency and with constant (independent of lateral

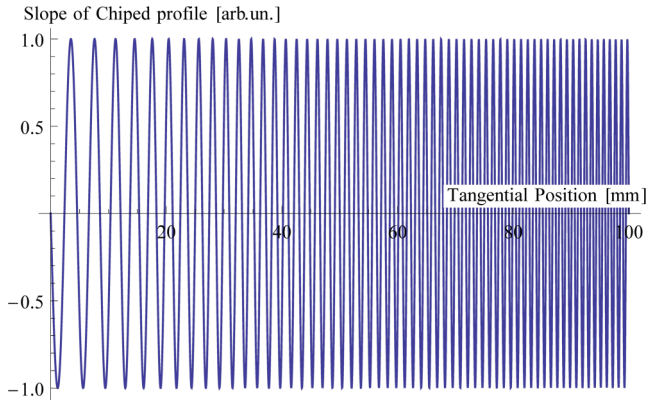

FIG. 3. Linear chirped slope profile (12) with the parameters: $A_0 = 1$, $\omega_1 = 0.004$ mm^{-2}, and $x_0 = 25$ mm.

position) slope amplitude as test artifacts for MTF calibration and resolution characterization of surface slope measuring profilers. In the height domain, the LCSPs are described with Fresnel functions with three parameters: A_0 is the slope variation amplitude in radians, ω_1 is the tangent parameter of linear variation of the spatial frequency in mm^{-2}, and x_0 is the offset of the lateral position in mm. The parameter x_0 has to provide the desired range of variation of the spatial frequency along the lateral position of the test sample. The range should include the spatial frequencies corresponding to the expected resolution of the instruments under test. Indirect measurements with a number of slope profilometers based on an electronic autocollimator[8,31] suggest a spatial resolution of about 1.7 mm. For the long trace profilers, the resolution is usually between 2 and 3 mm. Therefore, a suitable test sample should well cover the spatial wavelength range from $\lambda_{\min} \cong 1$ mm through $\lambda_{\max} \cong 5$ mm. This requirement can be transformed to the following conditions applied to the arguments of sin function in Eq. (12):

$$f_{\min} = \frac{1}{\lambda_{\max}} = \frac{d}{dx}\left[\omega_1 \cdot (x + x_0)^2\right]_{x_{\min}} = 2\omega_1(x_{\min} + x_0), \tag{13a}$$

$$f_{\max} = \frac{1}{\lambda_{\min}} = \frac{d}{dx}\left[\omega_1 \cdot (x + x_0)^2\right]_{x_{\max}} = 2\omega_1(x_{\max} + x_0). \tag{13b}$$

The parameters of such a profile are also limited by the technology applied to manufacture it. The lateral size we have chosen is 100 mm, which defines $x_{\max} = 100$ mm. Therefore, from Eqs. (13a) and (13b), $x_0 = 25$ mm and $\omega_1 = 0.004\ \mathrm{mm}^{-2}$. A profile with such parameters and $A_0 = 1$ rad is depicted in Figs. 2 and 3. Additionally the amplitude A_0 has to be large enough in order to minimize the perturbation of the calibration by different errors of slope measurements like random noise, systematic error, and errors due to temporal and temperature instabilities. For state of the art slope measuring profilers, the errors are significantly smaller than 1 μrad. Therefore a design consideration for A_0 is

$$A_0 \geq 10\ \mu\mathrm{rad}. \tag{14}$$

Realistic accuracy achievable for the fabrication process should also be taken into account. We assume that the accuracy is on a level of approximately 1 nm. Thus the amplitude of the height profile should be

$$h_0(x_{\max}) \geq 10\ \mathrm{nm}. \tag{15}$$

The amplitude in the height domain at $A_0 = 1$ rad (see Fig 2) is decreasing by a factor of ~5, from approximately $h_0(x_{\min}) \approx 0.75$ mm to $h_0(x_{\max}) \approx 0.16$ mm, when the lateral position is changing from $x_{\min} = 0$ mm through $x_{\max} = 100$ mm. Then the condition of Eq. (14) can be taken to set one more condition for the slope amplitude

$$A_0 \geq \frac{10\ \mathrm{nm}}{h_0(x_{\max}, A_0 = 1\ \mathrm{rad})} = \frac{10\ \mathrm{nm}}{0.16\ \mathrm{mm}} \approx 60\ \mu\mathrm{rad}. \tag{16}$$

Based on Eq. (16), we can choose the slope parameter to be

$$A_0 = 100\ \mu\mathrm{rad}. \tag{17}$$

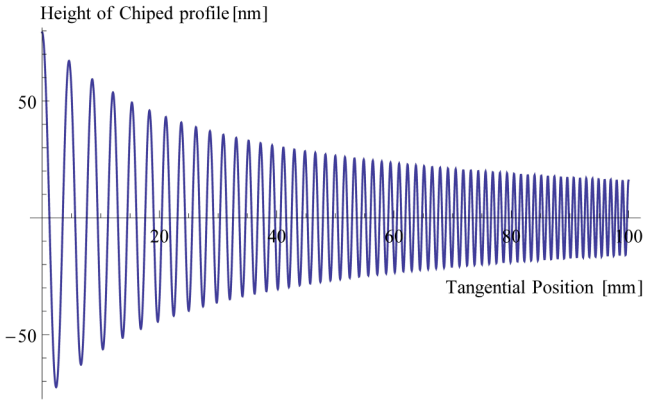

FIG. 4. Designed linear chirped slope profile shown in the height domain according parameters following Eqs. (17) and (16).

The corresponding chirped height profile is shown in the following Fig. 4.

The profile as shown in Fig. 4 was obtained by subtracting the middle line offset from Eq. (7)

$$h(x) = \frac{A_0}{2\sqrt{\omega_1}} \cdot \left\{S\left[2\sqrt{\omega_1} \cdot (x + x_0)\right] - S\left[\infty\right]\right\},\ S\left[\infty\right] = 1/2. \tag{18}$$

V. SAMPLE PREPARATION BY USE OF PLASMA JET MACHINING (PJM)—CONSIDERATIONS BETWEEN THEORY AND TECHNOLOGICAL LIMITATIONS

In order to manufacture a LCSP sample as specified in Sec. IV, several technological side conditions must be considered. First, a useful 2D representation of the LCSP must be generated. Since the profile is given as one-dimensional (1D) analytical formulae, a 2D topography on a discrete raster of approximately 100 mm in length (x), and 10 mm in width (y), and a pixel size of 0.01 mm has been numerically calculated using a Matlab® routine. The profile amplitude varies along the x direction while it remains constant in y (see Fig. 6).

The manufacturing of the given LCSP topography requires a sensitive and highly deterministic machining technology capable of resolving the fine spatial structures. Two surface finishing techniques that have proven to form a sufficiently small "tool tip" have been considered: ion beam figuring (IBF) and plasma jet machining (PJM).[29] Both techniques are well-developed for ultra-precision surface finishing. In either case, the surface is etched by an atomic particle beam that is moved over the surface by a Computerized Numerical Controlled (CNC) motion system. Depending on the local velocities applied, a certain amount of material is removed ending up in the desired surface profile. The beams generically exhibit rotationally symmetric Gaussian footprints, also called tool functions, which are characterized by a full width at half maximum (FWHM) and a maximum etching rate. The local scan velocity is determined by dwell time calculation algorithms, which, in general, perform a numerical de-convolution operation of the targeted surface topography and the tool function. The model function of the

dwell time method can be expressed as

$$h = R * t + \varepsilon, \tag{19}$$

where h is the resulting topography height, R is the tool function, t is the local dwell time (which is then converted to a velocity profile), and ε is the residual error.[29] The task of the dwell time simulation software is to calculate t and ε for a given h and R. The outcome of the simulation can be influenced by several parameters such as constant removal offset, maximum scan velocity, type of de-convolution algorithm, number of iterations, etc. Simple considerations regarding producibility of the given surface profile topographies start with the total amount of the material that has to be removed. Integrating the surface profile with respect to a horizontal plane that touches the profiles maximum yields the net volume to be etched, which is on the order of 0.075 mm^3. Since the CNC motion system has an upper velocity limit of 30 mm/s, zero removal cannot be realized at the profile maximum. Hence, a certain constant offset removal has to be added, which can be further increased by the simulation parameters. Obviously, the tool function FWHM wields the largest influence regarding the highest possible spatial resolution. Hence, it must correspond to the spatial dimensions of the smallest topographic features. Assuming a realistic tool function with a FWHM of 0.4–0.5 mm and reasonable machining times of approximately 2-3 h for such a topography, the required maximum etching rate of the tool can be estimated. In the present case, a volume material removal rate of approximately 0.05 mm^3/h is necessary. This implicates a center etching rate of the Gaussian tool function of ~50–70 nm/s. IBF is nowadays widely used in ultra-precision optics manufacturing as the final surface machining step. The material removal mechanism is based on physical sputtering by directing a low-energy argon ion beam (300 eV < E < 2000 eV) towards the surface. Due to its low removal rate of some nm/s, this technique is appropriate to correct surface figure errors to levels well below 1nm rms. IBF requires a vacuum environment.[35]

PJM is based on a plasma-assisted chemical removal process performed in normal atmosphere. Reactive species, generated in a RF driven plasma jet discharge, undergo reactions with surface atoms to form volatile compounds that are exhausted. In the case of silicon substrates, the plasma jet is fed by CF_4 as precursor gas to produce free fluorine radicals, which react to gaseous SiF_4. Generally, PJM provides significantly higher removal rates compared to IBF.[29] Typical IBF rates for a beam FWHM of 0.5 mm are in the order of 1-2 nm/s, whereas for PJM with comparable beam size, the etching rate lies between 50 and 80 nm/s. Obviously, the ion beam is not appropriate for machining the LCSP topographies. A more detailed analysis employing the dwell time simulation tools reveals the capability of the plasma jet tool to resolve the high frequency part of the LCSP for two of the three suggested profiles. Fig. 5 (left) shows the plasma jet discharge touching the silicon sample. In Fig. 5 (right), the plasma jet tool function cross section is depicted. Finally, an overall machining time for such topography was on the order of 3 h.

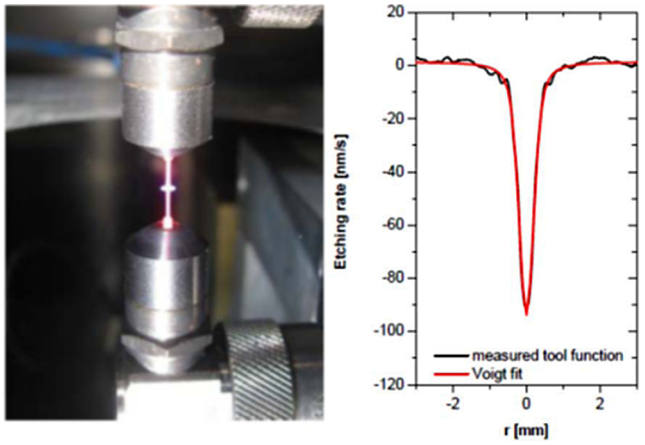

FIG. 5. Left: photograph of the plasma jet etching the silicon substrate. Right: plasma jet tool function cross section: FWHM = 0.465 mm, maximum etching 92 nm/s, volume-etching rate: 0.082 mm^3/h.

Figure 6 displays the chirped profile topography and the residual error (after subtraction of the corresponding desired profile from the simulated one) that were obtained by dwell time simulations and have been realized for this work. The residuals are negligible except the edge artefact, which is due to the van Cittert de-convolution algorithm used. In the center part, the peak-to-valley (pv) and rms values are

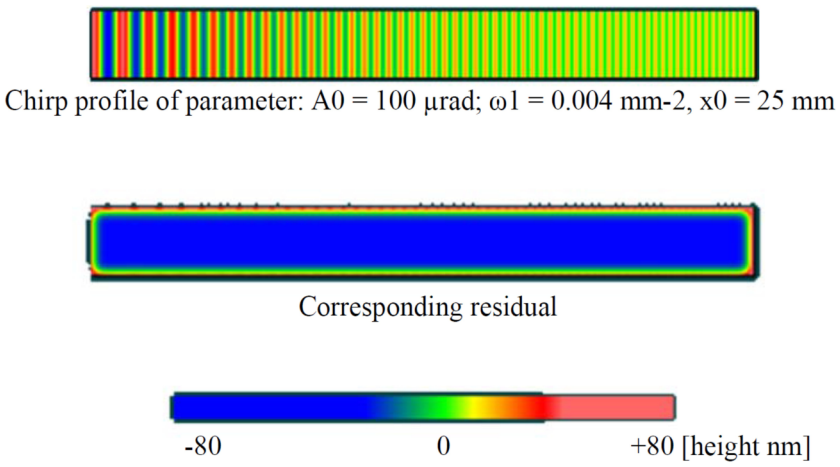

FIG. 6. Topography and residual errors (after subtraction of the desired profile from the measured one) of the chirp profile.

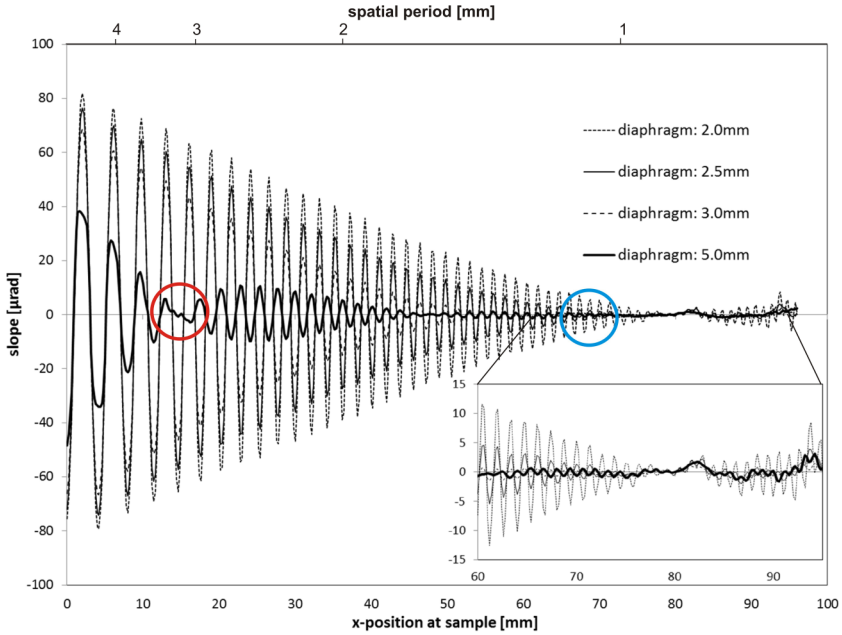

FIG. 7. Chirped surface profile in terms of surface slope as measured by use of the BESSY-NOM-autocollimator for different diaphragm diameter.

practically zero. As the sample substrate, a single-crystalline silicon slab with a diameter of 100 mm and a thickness of 10 mm has been chosen. This sample provides sufficient mechanical strength and heat conductivity, which is required for both stable manufacturing and measurement conditions. Furthermore, silicon is ideal for preparing a nearly sub-surface damage free flat and smooth surface by chemical-mechanical polishing. The initial long wavelength range figure error was less than 30 nm pv. The surface roughness has been determined to be in the order of <0.2 nm rms as measured with a white light interferometer (WLI).

VI. LCSP TEST SAMPLE MEASUREMENTS WITH BESSY NOM

First proof of principle tests for the above described profiles was performed with the BESSY-NOM,[5] an autocollimator based slope measuring profiler. A circular diaphragm was used to shape the measurement beam. The tests were performed with different aperture diameter of: 2.0, 2.5, 3.0, and 5.0 mm. The diaphragm was precisely aligned with respect to the autocollimator's optical axis.[36] The spacing between the diaphragm and the sample surface was about 3 mm. By scanning the NOM beam along the sample, slope traces with an increment of $\Delta x = 0.2$ mm were recorded in a step by step mode. Figure 7 shows the measured slope profiles of the samples with the length of 95 mm where the local spatial frequency varies from the low (at position $x_0 = 0$ mm) to the high (at position $x = 95$ mm) frequency.

The results in Fig. 7 can be used for direct extraction of the instrumental resolution. For this, the point of interest in the plot in Fig. 7, corresponding to the LCSP sample measurement with a certain size of the diaphragm, is the frequency where the slope oscillations reverse the phase. In Fig. 7, for the 5-mm-diaphragm trace, this place is depicted with a red circle. The corresponding spatial wavelength is 3.4 mm. For the 2.5 mm diaphragm, it is of 1.4 mm—see the blue circle. The physical origin of the phase reverse is the same as in the case of spoke resolution targets broadly used for resolution measurements with microscopes and interferometers (see, for example, Ref. 37. In the simplest case of a circular diaphragm and uniform light intensity distribution, the phase reverse corresponds to the change of sign of the MTF given by

$$MTF(u,v) = \frac{J_1\left(2\pi\, a\sqrt{u^2+v^2}\right)}{\pi\, a\sqrt{u^2+v^2}}, \tag{20}$$

where J_1 is the first order Bessel Function of the first kind, a is the diaphragm radius, and u and v are the orthogonal components of the spatial frequency f. The first zero of J_1 corresponds to $a\, f \cong 0.61$ or $\lambda_0 \cong a/0.61$. For example, with 5 mm diaphragm, this simple model predicts the NOM resolution cutoff at the wavelength of about 4.1 mm[31] that is in a reasonably good correspondence with the measured positions of the phase reverse. The 10%-15% difference between the measured cutoff wavelength and the one predicted with Eq. (20) is probably due to the rather complicated signal processing in the NOM autocollimator.

Practically, the profiler's MTF function can be reconstructed from the data in Fig. 7 by plotting the spatial frequency dependence of the amplitudes (with accounting the phase reversal as discussed above) of the envelope in the measured oscillating slope profile. Figure 8 depicts the dependence for the different beam shaping diaphragm sizes. The corresponding resolution cutoff wavelength (corresponding to the zero crossing) is about 3.4 mm for a 5 mm, 1.6 mm for the 3 mm, and 1.4 mm for the 2.5 mm diaphragm. Because of non-zero crossing of the 2.0 mm diaphragm curve, we are not able to give a value for this case. A more detailed description of processing of the data measured with LCSP sample, including consideration of MTF models for different instruments, is out of the scope of the present paper and will be discussed elsewhere.

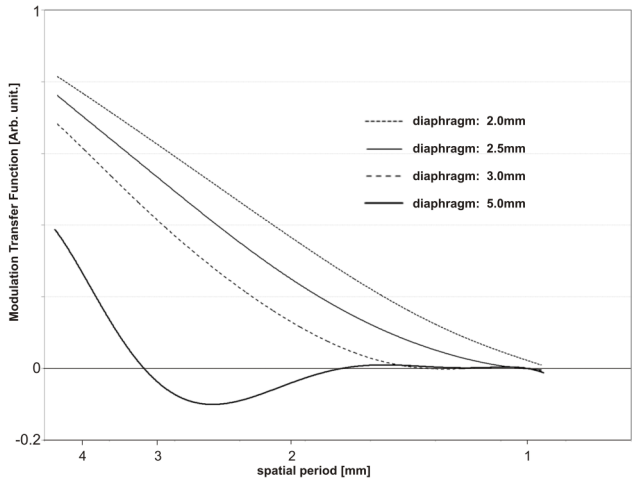

FIG. 8. MTF of the BESSY NOM equipped with beam shaping diaphragm of different diameter.

VII. CONCLUSION

We have suggested and investigated a new approach to the design of surface test profiles suitable for resolution (or MTF) calibration of different types of surface slope measuring profilometers. The new approach incorporates practical requirements that profiles obey constant amplitude of slope variation with a linear variation of spatial frequency along its lateral position. The proof of principle tests with the developed LCSP samples was performed with the BESSY NOM, an autocollimator based slope profiler with different diameters of the beam limited diaphragm: 2.0, 2.5, 3.0, and 5.0 mm. We have discussed the effects of a phase-reversal in the measured slope profiles that can be easily identified and used to provide an immediate measure of the instrument's spatial resolution. Compared to previous work,[31,34] the results of the present measurements show a slightly higher spatial resolution determined here as a high spatial frequency cutoff (position of the phase reverse). This can be due to the large slope amplitude of the developed LCSP, so that the instrumental noise level does not affect the measured resolution. Different from the approach discussed in Ref. 31, we have chosen here a profile with a maximum amplitude (peak-to-valley) of 150 nm, which is optimal for the spatial resolution calibration of a slope measuring profiler. Such a deep test profile can have some drawbacks due to very large local curvature that appears to be less than 3 m at the higher frequency range. The real X-ray optical components usually do not have such high figure variation at spatial frequencies close to the resolution cut-off, and correspondingly, the slope profilers, such as the BESSY-NOM, are designed to measure optics of minimum 5 m local curvature. The strong local curvature and its change from convex to concave can impact the performance of the calibration of a profiler via shaping the measurement. Nevertheless, as it is shown in Sec. VI, the developed LCSP test sample provides very reliable information on the instrument's MTF. In the next generation of the LCSP sample, we are going to address this potential problem. An important point is that a MTF calibration of a slope measuring profiler does not directly have an effect on the accuracy of measurements of a surface slope profile. Rather, it provides reliable data on the instrument resolution and the spatial bandwidth of the measurements. However, in the spatial frequency domain, when the surface power spectral density (PSD) is measured, the MTF calibration can be directly applied to eliminate the instrumental effect on the surface PSD data.

In conclusion, we have demonstrated that the suggested approach to the MTF calibration of slope profilers, based on application of LCSP test samples, is capable of providing solid information on the spatial frequency range of NOM- and LTP-like surface slope measuring profilometers that are currently in use at synchrotron and X-ray astronomy facilities around the world. The information about the instrument's MTF is also of fundamental importance for metrology used during optical fabrication, especially when deterministic surface finishing is applied on the basis of the measured surface topography data. As the next step, we are working on the development of LCSP samples suitable for calibration of prospective instruments with a resolution below 0.5 mm. In upcoming publications, we plan to investigate the impact of modified diaphragm geometry like square or rectangular base for shaping the measurement beam for different experimental arrangements.

ACKNOWLEDGMENTS

The authors are grateful to Daniel Merthe, Wayne McKinney, and Gary Centers (all with the Lawrence Berkeley National Laboratory) for useful discussions. The work of F. Siewert was partially funded by the European Metrology Research Project No. EMRP-JRP SIB58 Angles within the EURAMET program of the European Union. Research at the Advanced Light Source is supported by the Director, Office of Science, Office of Basic Energy Sciences, Material Science Division of the U.S. Department of Energy under Contract No. DE-AC02-05CH11231 at Lawrence Berkeley National Laboratory.

[1]H. Wolter, "Spiegelsysteme streifenden Einfalls als abbildende Optiken für Röntgenstrahlen," Ann. Phys. **445**, 94 (1952).
[2]P. Kirkpatrick and A. V. Baez, "Formation of optical images by x-rays," J. Opt. Soc. Am. **38**, 9 (1948).
[3]P. Takacs, S. N. Qian, and J. Colbert, "Design of a long trace surface profiler," Proc. SPIE **749**, 59–64 (1987).
[4]S. Qian, W. Jark, and P. Z. Takacs, "The pentaprism LTP—A long trace profiler with stationary optical head and moving penta prism," Rev. Sci. Instrum. **66**(3), 2562-2569 (1995).
[5]F. Siewert, T. Noll, T. Schlegel, T. Zeschke, and H. Lammert, "The nanometer optical component measuring machine: A new sub-nm topography measuring device for x-ray optics at BESSY," AIP Conf. Proc. **705**, 847–850 (2004).
[6]F. Siewert, J. Buchheim, T. Zeschke, M. Störmer, G. Falkenberg, and R. Sankari, "On the characterization of ultra-precise x-ray optical components: Advances and challenges in *ex situ* metrology," J. Synchrotron Radiat. **21**, 968–975 (2014).
[7]F. Siewert *et al.*, "Advanced metrology: An essential support for the surface finishing of high performance x-ray optics," Proc. SPIE **5921**, 592101 (2005).
[8]V. V. Yashchuk, S. Barber, E. E. Domning, J. L. Kirschman, G. Y. Morrison, B. V. Smith, F. Siewert, T. Zeschke, R. Geckler, and A. Just, "Sub-microradian surface slope metrology with the ALS developmental long trace profiler," Nucl. Instrum. Methods Phys. Res., Sect. A **616**, 212–223 (2010).
[9]S. G. Alcock, K. J. S. Sawhney, S. Scott, U. Pedersen, R. Walton, F. Siewert, T. Zeschke, T. Noll, and H. Lammert, "The diamond-NOM:

A non-contact profiler capable of characterizing optical figure error with sub-nm repeatability," Nucl. Instrum. Methods Phys. Res., Sect. A **616**, 224–228 (2010).
[10]J. Nicolas and J. C. Martinez, "Characterization of the error budget of Alba-NOM," Nucl. Instrum. Methods Phys. Res., Sect. A **710**, 24 (2013).
[11]L. Assoufid, N. Brown, D. Crews, J. Sullivan, M. Erdmann, J. Qian, P. Jemian, V. V. Yashchuk, P. Z. Takacs, N. A. Artemiev, D. J. Merthe, W. R. McKinney, F. Siewert, and T. Zeschke, "Development of a high-performance gantry system for a new generation of optical slope measuring profilers," Nucl. Instrum. Methods Phys. Res., Sect. A **710**, 31 (2013).
[12]S. Qian, L. Wayne, and M. Idir, "Nano-accuracy measurements and the surface profiler by use of Monolithic Hollow Penta-Prism for precision mirror testing," Nucl. Instrum. Methods Phys. Res., Sect. A **759**, 224–228 (2014).
[13]R. D. Geckeler and I. Weingärtner, "Sub-nm topography measurement by deflectometry: Flatness standard and wafer nanotopography," Proc. SPIE **4779**, 1–12 (2002).
[14]Z. Ali, N. A. Artemiev, C. L. Cummings, E. E. Domning, N. Kelez, W. R. McKinney, D. J. Merthe, G. Y. Morrison, B. V. Smith, and V. V. Yashchuk, "Automated suppression of errors in LTP-II slope measurements with x-ray optics," Proc. SPIE **8141**, 81410O (2011).
[15]Y. Senba, H. Kishimoto, H. Ohashi, H. Yumoto, T. Zeschke, F. Siewert, S. Goto, and T. Ishikawa, "Upgrade of long trace profiler for characterization of high-precision x-ray mirrors at SPring-8," Nucl. Instrum. Methods Phys. Res., Sect. A **616**(2-3), 237–240 (2010).
[16]M. Thomasset, S. Brochet, and F. Polack, "Latest metrology results with the SOLEIL synchrotron LTP," Proc. SPIE **5921**, 592102 (2005).
[17]A. Rommeveaux, O. Hignette, and C. Morawe, "Mirror metrology and bender characterization at ESRF," Proc. SPIE **5921**, 59210N (2005).
[18]F. Siewert, J. Buchheim, S. Boutet, G. Williams, P. A. Montanez, J. Krzywinski, and R. Signorato, "Ultra-precise characterization of LCLS hard x-ray focussing mirrors by high resolution slope measuring deflectometry," Opt. Express **20**(4), 4525–4536 (2012).
[19]H. Mimura, S. Morita, T. Kimura, D. Yamakawa, W. Lin, Y. Uehara, S. Matsuyama, H. Yumoto, H. Ohashi, K. Tamasaku, Y. Nishino, M. Yabashi, T. Ishikawa, H. Ohmori, and K. Yamauchi, "Focusing mirror for x-ray free electron lasers," Rev. Sci. Instrum. **79**, 083104 (2008).
[20]F. Siewert, J. Buchheim, T. Zeschke, G. Brenner, S. Kapitzki, and K. Tiedtke, "Sub-nm accuracy metrology for ultra-precise reflective x-ray optics," Nucl. Instrum. Methods Phys. Res., Sect. A **635**, 52–57 (2011).
[21]M. Idir, K. Kaznatcheev, G. Dovillaire, J. Legrand, and R. Rungsawang, "A 2 D high accuracy slope measuring system based on a stitching Shack Hartmann optical head," Opt. Express **22**(3), 2770 (2014).
[22]V. Yashchuk, W. McKinney, T. Warwick, T. Noll, F. Siewert, T. Zeschke, and R. Geckeler, "Proposal for a universal test mirror for characterization of slope measuring instruments, advances in metrology for x-ray and EUV optics II," Proc. SPIE **6704**, 67040A (2007).
[23]F. Siewert, J. Buchheim, and T. Zeschke, "Calibration and characterization of 2nd generation slope measuring profiler," Nucl. Instrum. Methods Phys. Res., Sect. A **616**, 119–127 (2010).
[24]V. V. Yashchuk, N. A. Artemiev, I. Lacey, W. R. McKinney, and H. A. Padmore, "Advanced environmental control as a key component in the development of ultra-high accuracy ex situ metrology for x-ray optics," Opt. Eng. **54**(9), 104104 (2015).
[25]S. Roling *et al.*, "Time-dependent wave front propagation simulation of a hard x-ray split-and-delay unit: Towards a measurement of the temporal coherence properties of x-ray free electron lasers," Phys. Rev. Spec. Top.–Accel. Beams **17**, 110705 (2014).
[26]L. Samoylova *et al.*, "Requirements on hard x-ray grazing incidence optics for European XFEL: Analysis and simulation of wavefront transformations," Proc. SPIE **7360**, 73600E5 (2009).
[27]A. Schindler *et al.*, "Finishing procedure for high performance synchrotron optics," Proc. SPIE **5180**, 64–72 (2003).
[28]H. Thiess, H. Lasser, and F. Siewert, "Fabrication of x-ray mirrors for synchrotron applications," Nucl. Instrum. Methods Phys. Res., Sect. A **616**(2–3), 157–161 (2010).
[29]T. Arnold *et al.*, "Ultra-precision surface finishing by ion beam and plasma jet techniques: Status and outlook," Nucl. Instrum. Methods Phys. Res., Sect. A **616**(2–3), 147–156 (2010).
[30]P. Rose, Y. Surrel, and J. M. Becker, Meas. Sci. Technol. **20**, 095110 (2009).
[31]F. Siewert, J. Buchheim, T. Höft, T. Zeschke, A. Schindler, and T. Arnold, "Investigations on the spatial resolution of autocollimator—Based slope measuring profilers," Nucl. Instrum. Methods Phys. Res., Sect. A **710**, 42–47 (2013).
[32]S. C. Irick, Rev. Sci. Instrum. **63**, 1 (1992).
[33]F. Siewert, "Slope error and surface roughness," in *Modern Developments in X-ray and Neutron Optics* (Springer, 2008).
[34]Y. V. Yashchuk and V. V. Yashchuk, "Reliable before-fabrication forecasting of expected surface slope distributions for x-ray optics," Opt. Eng. **51**(4), 046501 (2012).
[35]Th. Arnold, G. Boehm, and H. Paetzelt, "Ultra-precision surface machining with reactive plasma jets," Contrib Plasma Phys. **54**, 145–154 (2014).
[36]R. D. Geckeler, N. A. Artemiev, S. K. Barber, A. Just, O. Kranz, I. Lacey, F. Siewert, B. V. Smith, and V. V. Yashchuk, "Aperture use and alignment in autocollimator-based deflectometric profilometers," in Abstract to The International Workshop on Metrology for X-ray Optics, Mirror Design, and Fabrication, Satellite Workshop at the 12th International Conference on Synchrotron Radiation Instrumentation, SRI 2018, Berkeley, USA, 13–16 July 2015, the corresponding paper has been submitted to Rev. Sci. Instrum.
[37]G. D. Boreman, *Modulation Transfer Function in Optical and Electro-optical Systems* (SPIE Press, Bellingham, Washington, 2001).